ACS APPLIED MATERIALS & INTERFACES

Letter

www.acsami.org

Structural Improvement of $CaFe_2O_4$ by Metal Doping toward Enhanced Cathodic Photocurrent

Keita Sekizawa,[†,‡] Takamasa Nonaka,[†] Takeo Arai,[†,‡] and Takeshi Morikawa*[,†,‡]

[†]Toyota Central Research & Development Laboratories, Inc., 41-1, Yokomichi, Nagakute, Aichi 480-1192, Japan

[‡]Advanced Catalytic Transformation Program for Carbon Utilization (ACT-C), Japan Science and Technology Agency, 4-1-8 Honcho, Kawaguchi, Saitama 332-0012, Japan

Supporting Information

ABSTRACT: Various metal-doped *p*-type $CaFe_2O_4$ photocathodes were prepared in an attempt to improve the low quantum efficiency for photoreaction. CuO and Au doping enhanced the photocurrent by expansion of the absorption wavelength region and plasmon resonance, respectively. X-ray diffraction (XRD) and X-ray absorption fine structure (XAFS) analysis showed that doping with these metals further disturbed the originally distorted crystal structure of $CaFe_2O_4$. In contrast, doping with Ag relaxed the distorted crystal structure around the Fe center toward symmetry. Ag doping resulted in improvement of the carrier mobility together with a red-shift of photoabsorption with Ag-doped $CaFe_2O_4$ having a 23-fold higher photocurrent than undoped $CaFe_2O_4$.

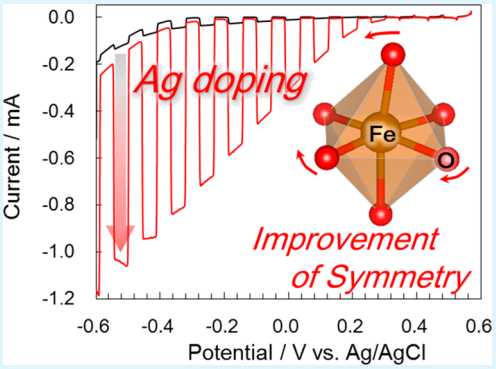

KEYWORDS: *earth-abundant materials, p-type semiconductor, X-ray absorption fine structure, ferrite compound, thin film*

Photocatalytic reactions are widely used for solar energy conversion[1] and environmental purification,[2] and they require semiconductors which show efficient photoresponses owing to their narrow bandgaps, high carrier densities, and mobility. To realize efficient photocatalytic systems, reports on combinations of *p*-type and *n*-type semiconductors for photoelectrochemical devices[3−6] and photocatalysts[7−9] have been increasing. Although there have been many reports on highly efficient *n*-type semiconductors, there have been comparatively few studies on *p*-type semiconductors, most of which consist of rare metals. Hence development of efficient *p*-type semiconductors is crucial. Calcium iron oxide ($CaFe_2O_4$) is an attractive *p*-type semiconductor which consists of only abundant elements. $CaFe_2O_4$ exhibits visible-light response (bandgap = 1.9 eV) and a suitable conduction band edge (−0.6 V vs RHE)[10] for application to water splitting,[11,12] photodecomposition of harmful organics,[13] and superhydrophilic reactions.[14] However, the quantum efficiency of the $CaFe_2O_4$ electrode is relatively low, which is mainly due to its poor mobility (ca. 10^{-1} V^{-1} s^{-1} cm^2).[15]

Metal doping into metal oxide has often been attempted to induce a red-shift of the bandgap transition[1] and generate acceptor levels in the bandgap due to enhanced *p*-type character.[16] Furthermore, if the atomic orbitals of the dopant are hybridized with the narrow d band in the conduction band (CB) or valence band (VB), bandgap modulation and an enhancement of carrier mobility are expected.

Here, to explore a suitable dopant, we have prepared various metal-doped $CaFe_2O_4$ (M-$CaFe_2O_4$; M = Ag, Au, CuO, Pd, and Ir) electrodes by radio frequency (RF) magnetron cosputtering followed by postannealing at a low temperature. It was confirmed that some metals enhance the photoelectrochemical properties of $CaFe_2O_4$. The enhancement effects of the cationic dopants were investigated in detail by structural analyses.

$CaFe_2O_4$ and a metal were codeposited by RF magnetron sputtering onto glass substrates coated with antimony-doped tin oxide (ATO), a transparent conductive oxide. The compositions of the films were adjusted by changing the input RF powers for the metal target in the range of 0−300 W, while that for $CaFe_2O_4$ was fixed at 500 W. The film thickness was adjusted to ca. 180 nm according to the sputtering time. The deposited electrodes were postannealed at an optimum temperature of 923 K in an O_2 gas flow for 2 h. The surface of the films was confirmed to be flat as shown by the scanning electron microscopy (SEM) image (Figure S1, Supporting Information). Representative scanning transmission electron microscopy (STEM) images (Figure S2e, Supporting Information) revealed that metals were aggregated in the films after annealing, while there were no aggregates before annealing (Figure S2d, Supporting Information). It indicates that an excess amount of metals for doping in lattices of $CaFe_2O_4$ aggregated during the annealing process.

Current−potential curves of the sputter-deposited films were measured in an electrochemical cell containing O_2-saturated 0.2

Received: April 24, 2014
Accepted: July 1, 2014
Published: July 1, 2014

M K_2SO_4 aqueous solution equipped with Pt wire and Ag/AgCl electrodes. In all of M-$CaFe_2O_4$'s, only Ag-$CaFe_2O_4$ showed dark current, which is a redox wave of Ag/Ag^+ by the elution of aggregated Ag. After oxidation by chronoamperometry at 0.6 V vs Ag/AgCl, the current disappeared, as shown in Figure S3 (Supporting Information). After this treatment, the color of the film changed from dark brown to yellow (Figure S3, Supporting Information), and voids due to the elution of Ag were evident by STEM analysis (Figure S2f, Supporting Information). Energy-dispersive X-ray (EDX) spectroscopy measurements indicated the residual amount of Ag was less than the detectable limit (<0.5 atom %). After repeated washing of the electrodes with distilled water, photocurrent−voltage curves were measured with fresh electrolyte.

Figure 1 shows current−potential curves for the Ag, CuO, Au, and undoped $CaFe_2O_4$ electrodes under chopped light

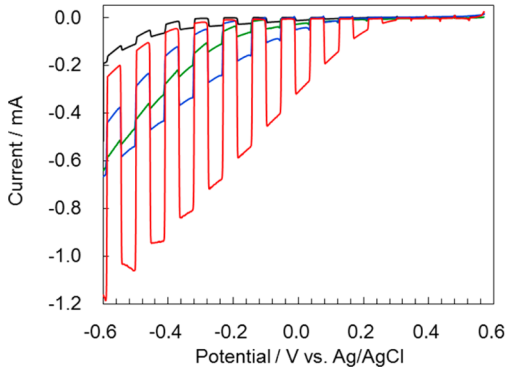

Figure 1. Current−potential curves measured in O_2-saturated 0.2 M K_2SO_4 solution under chopped light irradiation (300−800 nm) for Ag (35 W)-$CaFe_2O_4$ (red line), CuO (300 W)-$CaFe_2O_4$ (blue line), Au (50 W)-$CaFe_2O_4$ (green line), and $CaFe_2O_4$ (black line) electrodes. All electrodes were postannealed at 927 K, and the film thickness was fixed at ca.180 nm.

irradiation. These films exhibit typical cathodic photocurrents that correspond to O_2 reduction, which indicates that M-$CaFe_2O_4$'s are also *p*-type semiconductors. Ag (35 W)-$CaFe_2O_4$ (red line) showed the highest photoactivity. The photocurrent at 0.0 V vs Ag/AgCl was 23 times higher than that for $CaFe_2O_4$ (black line). Other Ag-$CaFe_2O_4$'s prepared by RF sputtering of a silver target in the range of 20−60 W also showed a higher photocurrent than $CaFe_2O_4$ (Figure S4a, Supporting Information). CuO-$CaFe_2O_4$ deposited by cosputtering with a RF power of 50−300 W for CuO also exhibited 1.3−2.9 times higher photocurrent than that of $CaFe_2O_4$ at 0 V (Figure S4b, Supporting Information). The photocurrent for Au (50 W)-$CaFe_2O_4$ was 1.7 times higher than that of $CaFe_2O_4$, although those for the Au electrodes sputtered at 15−37 W were lower (Figure S4c, Supporting Information). In contrast, doping with Pd and Ir did not enhance the photocurrent of $CaFe_2O_4$ (Figures S4d, e, Supporting Information). Time courses for the photocurrents with a bias of 0 V are shown in Figure S5 (Supporting Information). Although the photocurrents for CuO-$CaFe_2O_4$ and Au-$CaFe_2O_4$ decreased, that of Ag-$CaFe_2O_4$ was stable.

Figure 2 shows UV−vis absorption and incident photon to current efficiency (IPCE) spectra for $CaFe_2O_4$ doped with Ag, CuO, and Au and undoped $CaFe_2O_4$ films. The absorption edge of $CaFe_2O_4$ (ca. 650 nm, black line) was shifted to the longer-wavelength region by doping with Ag and CuO (red and

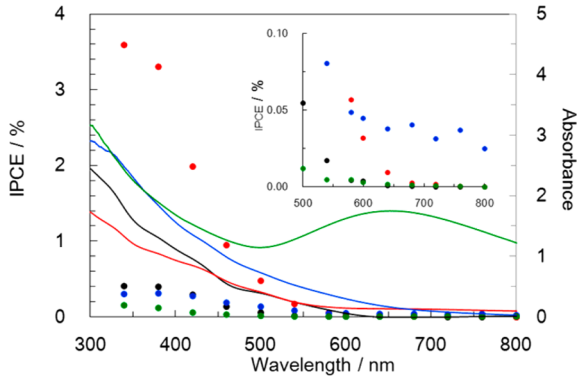

Figure 2. IPCE spectra (data points; left axis) and UV−vis absorption spectrum (lines; right axis) for Ag (35 W)-$CaFe_2O_4$ (red), CuO (300 W)-$CaFe_2O_4$ (blue), Au (50 W)-$CaFe_2O_4$ (green), and $CaFe_2O_4$ (black) electrodes. IPCEs were measured at 0.0 V vs Ag/AgCl with monochromatic light irradiation. The film thicknesses of all electrodes were fixed at ca.180 nm.

blue lines, respectively). The Au-$CaFe_2O_4$ film showed not only a red-shift but also an absorption peak around 500−800 nm (green line) which is attributed to the plasmonic absorption of Au nanoparticles.

The IPCE spectra also shifted toward the longer-wavelength region, which corresponds to the red-shift of the absorption edge with doping. The photocurrent of $CaFe_2O_4$ was obtained at less than 600 nm, while that of Ag-, Au-, and CuO-$CaFe_2O_4$ was observed at 720 nm (Figure S6, Supporting Information). Therefore, it is speculated that cationic Ag, Cu, and Au may be introduced into the $CaFe_2O_4$ lattice to create a new level between the VB and/or CB in the bandgap. In the case of CuO-$CaFe_2O_4$, enhanced photoresponse was observed at longer wavelengths of 460−800 nm. The improvement of photocurrent by full-arc irradiation in Figure 1 is considered to be due to the improved photoresponse between 460 and 800 nm. However, the IPCE below 420 nm is lower than that for $CaFe_2O_4$, which indicates that CuO doping has not only a positive effect by the bathochromic shift but also a negative effect in the generation of electron and hole trap sites.[1] In the case of Au-$CaFe_2O_4$, the IPCE was lower than that of $CaFe_2O_4$ below 600 nm. A decrease of photocurrent should also be caused by the generation of trap sites with Au doping. However, this is contradicted by the 70% increase in photoresponse with full-arc irradiation (Figure 1). This result indicates that the improved photocurrent for Au-$CaFe_2O_4$ requires multicolor irradiation, i.e., excitation to both bandgap and Au plasmons. It is a possibility that the improved photocurrent may be due to localized surface plasmon resonance (LSPR) by Au plasmons.[17] Photoexcitation of the LSPR peak is known to form a locally enhanced electric field in the proximity of metal nanoparticles, which can then enhance the photoexcitation of chromophores near the metal nanoparticles. In the case of Au-$CaFe_2O_4$, the electric field induced by photoexcitation of the LSPR peak for Au nanoparticles (λ > 500 nm) may enhance the photoexcitation of $CaFe_2O_4$ (λ < 600 nm). Despite that Au acts as a trap site, the photocurrent by full-arc irradiation may be increased. In contrast, the IPCE for Ag-$CaFe_2O_4$ was much higher than that for $CaFe_2O_4$ over the entire wavelength region. Therefore, doping with Ag is effective not only for the absorption red-shift but also for an improvement of the photoresponse in the range of 340−760 nm. As reasons for photocurrent enhancement, Ag doping may

dx.doi.org/10.1021/am502500y | *ACS Appl. Mater. Interfaces* 2014, 6, 10969−10973

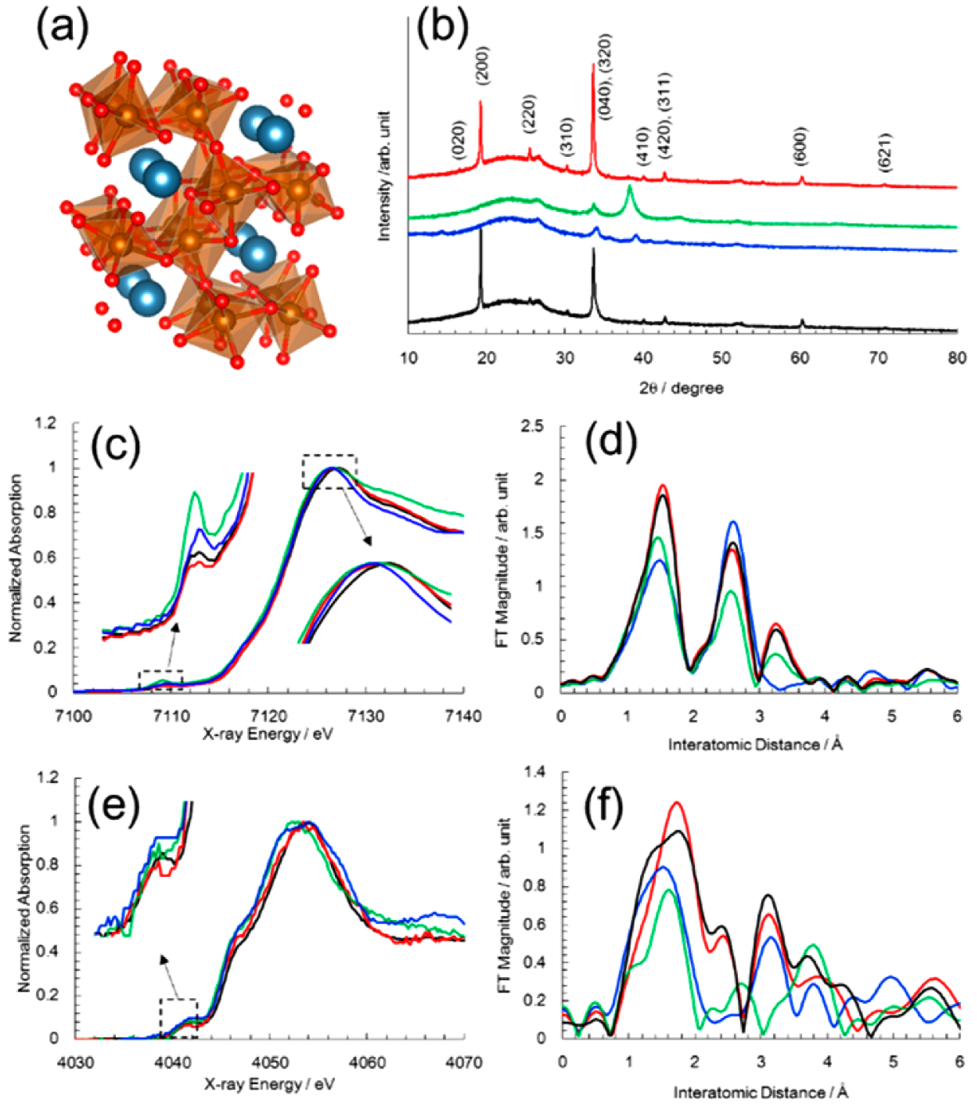

Figure 3. (a) Crystal structure of $CaFe_2O_4$ (Ca, blue; Fe, brown; O, red), (b) XRD patterns, and XANES and k^2-weighted FT-EXAFS spectra for Fe K-edge (c and d, respectively) and that for Ca K-edge (e and f, respectively) of Ag-$CaFe_2O_4$ (red), CuO-$CaFe_2O_4$ (blue), Au-$CaFe_2O_4$ (green), and $CaFe_2O_4$ (black) electrodes.

promote reaction with O_2 at the surface or improve bulk properties such as the carrier mobility.

To investigate the effect of Ag-doped sites and Ag particles for the reaction, a $CaFe_2O_4$ electrode loaded with Ag nanoparticles [Ag particle/$CaFe_2O_4$/ATO] and a Ag-doped $CaFe_2O_4$ electrode layer [Ag-$CaFe_2O_4$/$CaFe_2O_4$/ATO] were prepared. Photoinduced current−potential curves of these electrodes are shown in Figure S7 (Supporting Information), where the photocurrents of both electrodes were degraded. These results indicate that Ag-doped sites and Ag particles do not act as reduction sites to enhance the photocurrent in Ag-$CaFe_2O_4$.

To examine the bulk properties of Ag-$CaFe_2O_4$, the dependence of photocurrent on the film thickness was investigated. Photocurrent−voltage curves of 100−500 nm thick Ag-$CaFe_2O_4$ and $CaFe_2O_4$ films are shown in Figure S8 (Supporting Information). For $CaFe_2O_4$, the best photocurrent obtained at −0.25 V vs Ag/AgCl was for the 100 nm film and then decreased with increasing film thickness. The short carrier diffusion length in $CaFe_2O_4$ resulted in poor photoelectrochemical properties. This is disadvantageous for efficient light absorption because the majority of incident photons is transmitted through the thin film. In contrast, the optimum thickness of the Ag-$CaFe_2O_4$ film was 230 nm, and an efficient photocurrent was observed even at 500 nm. Therefore, more photons were absorbed in the thicker Ag-$CaFe_2O_4$ films, which can be explained by more photogenerated holes reaching the transparent electrode with improved carrier mobility. The enhancement of carrier mobility by Ag doping was estimated to be 4.6 times (Supporting Information). Consequently, the enhancement of the photoresponse with Ag doping is considered due to an improvement of the carrier mobility in the bulk. A detailed crystallographic analysis was then conducted to investigate the factors for improvement of the bulk properties with doping.

Figure 3b shows XRD patterns for Ag-, CuO-, and Au-doped $CaFe_2O_4$ and undoped $CaFe_2O_4$ electrodes. The undoped $CaFe_2O_4$ electrode has two intense peaks assignable to (200) and the overlap of (040) and (320), in addition to several weak peaks. Ag-$CaFe_2O_4$ also had intense peaks similar to that for $CaFe_2O_4$. The intensity of the (200) diffraction peak for Ag-$CaFe_2O_4$ was decreased slightly, while the other several peaks

dx.doi.org/10.1021/am502500y | ACS Appl. Mater. Interfaces 2014, 6, 10969−10973

were increased and shifted to lower angle by $\Delta 2\theta = 0.02-0.03°$ (Figure S10, Supporting Information). This indicates that doping with Ag induces a change of the crystal orientation in the film structure and the lattice spacing. In contrast, all of the peak intensities for the Au- and CuO-doped electrodes were decreased, and other peaks assignable to Au ($2\theta = 38.2°$) and CuO ($2\theta = 38.9°$) were observed. Films doped with Pd and Ir also showed a significant decrease in the $CaFe_2O_4$ peaks and the appearance of metallic phase dopant peaks.

XAFS spectra for the K-edge of Ca and Fe were measured to probe the short-range structure.[18] However, we could not obtain information on Ag because the dopant amounts were below the detection limit (less than 0.5 atom %). Figure 3c shows Fe K-edge X-ray absorption near edge structure (XANES) spectra for metal-doped $CaFe_2O_4$. Pre-edge peaks and absorption peaks were observed around 7109 and 7127 eV, respectively. The absorption maxima of Ag-$CaFe_2O_4$ were shifted to lower energy than that of $CaFe_2O_4$, which indicates that the electronic structure of Fe became reductive by Ag doping. The pre-edge peak of Ag-$CaFe_2O_4$ is lower than that of $CaFe_2O_4$ and is attributed to forbidden transitions such as 1s → 3d, which is allowed by degradation of the ligand-field symmetry around Fe due to p-character mixing with d orbitals. Therefore, the difference in the pre-edge peak indicates that Ag doping induces improvement of the symmetry around the Fe atom in $CaFe_2O_4$. In contrast, Au and CuO doping caused disturbance of the symmetry.

Figure 3d shows the Fourier transforms (FTs) of k^2-weighted extended X-ray absorption fine structure (EXAFS) spectra, which were collected for specific nearest-neighbor interatomic distances. The FT-EXAFS data showed three major peaks. $CaFe_2O_4$ has a distorted spinel structure (Figure 3a),[19] in which each Fe atom is surrounded by six O atoms in octahedral coordination. The first shell peak of the FT-EXAFS signal at ca. 1.6 Å is assigned to families of O atoms. The second shell peak at ca. 2.7 Å is assigned to single scattering by Fe−Ca and Fe−Fe atoms, while the third shell peak at ca. 3.2 Å represents contributions from both Ca, Fe, and O atoms. In the case of Ag-$CaFe_2O_4$, the FT magnitude of the first peak was higher than that of $CaFe_2O_4$, which also indicates improvement of the symmetry around Fe. The peak of the first shell was slightly shifted to longer interatomic distance with Ag doping. In contrast, the first shell shifted shorter, and the FT magnitude was lowered with Au and CuO doping.

The Ca K-edge XANES and FT-EXAFS spectra for metal-doped $CaFe_2O_4$ are shown in Figures 3e and 3f, respectively. These spectra contain much noise because the energy of the Ca K-edge is weak. The difference in the pre-edge and the absorption edge energy by doping could not be recognized. The FT-EXAFS data showed three major peaks. The first shell between 1.7 and 2.0 Å is attributed to single scattering by the surrounding eight O atoms. The other shells contain various scattering by Ca, Fe, and O atoms. The peak intensity of the first shell for Ag-$CaFe_2O_4$ is higher than that for $CaFe_2O_4$, which indicates the symmetry around Ca is also improved by Ag doping. In contrast, the first shell peak was more split and lowered by Au and CuO doping, which is considered to be because the symmetry of the Ca−O bond is lowered.

Decreasing symmetry is closely related to carrier mobility because mobility is highly dependent on the overlap of atomic orbitals. The CB minimum of $CaFe_2O_4$ consists of the Fe 3d, while the VB is mainly composed of Fe 3d and O 2p.[20,21] Therefore, the orbital overlap of the 3d orbitals of Fe with the 2p orbital of O^{2-} is important for the carrier mobility. The overlap must be significantly reduced by decreasing symmetry around Fe because of the narrow and anisotropic 3d orbital. Therefore, the low mobility is closely related to the distorted lattice structure. Doping with Ag induces an improvement in the symmetry around the central Fe atom. The structural improvement may also induce high mobility, which is considered to be the main reason for the significantly high photocurrent. These results introduce a new strategy for the formation of highly efficient semiconductor materials. This structural change by Ag doping may be applicable to other distorted oxide semiconductors.

In conclusion, various metal-doped $CaFe_2O_4$ semiconductors with *p*-type conductivity were produced by RF magnetron cosputtering. Doping of CuO, Au, and Ag resulted in an enhancement of the photocurrent. Although CuO and Au doping enhanced photocurrent by expansion of the absorption wavelength and plasmon resonance, respectively, the doping decreased the symmetry around the Fe center and the crystallinity of $CaFe_2O_4$. In contrast, Ag doping relaxed the distorted crystal structure of $CaFe_2O_4$ together with a red-shift in photoabsorption. As a result, Ag-doped $CaFe_2O_4$ exhibited 23 times higher photocurrent than undoped $CaFe_2O_4$. Ag-$CaFe_2O_4$ would be economically desirable as photocatalysts for environmental purification[13] and superhydrophilic reactions[14] and solar energy conversion[5,11,12] by conjugating *n*-type semiconductor since it is composed of naturally abundant elements.

■ ASSOCIATED CONTENT

Ⓢ Supporting Information

General procedures, photoelectrochemical property, and SEM and TEM images. This material is available free of charge via the Internet at http://pubs.acs.org.

■ AUTHOR INFORMATION

Corresponding Author

*E-mail: morikawa@mosk.tytlabs.co.jp.

Notes

The authors declare no competing financial interest.

■ ACKNOWLEDGMENTS

The authors thank Mai Asaoka, Kousuke Kitazumi, Naoko Takahashi, Toyokazu Nomoto, Masakazu Kanechika, and Keiichiro Oishi for assistances in the experiments. The Fe K-edge XAFS measurements were performed at the BL33XU of SPring-8 with the approval of the Japan Synchrotron Radiation Research Institute (JASRI) (Proposal No. 2013B7022).

■ REFERENCES

(1) Kudo, A.; Miseki, Y. Heterogeneous Photocatalyst Materials for Water Splitting. *Chem. Soc. Rev.* **2009**, *38* (1), 253−78.

(2) Hoffmann, M. R.; Martin, S. T.; Choi, W.; Bahnemann, D. W. Environmental Applications of Semiconductor Photocatalysis. *Chem. Rev.* **1995**, *95* (1), 69−96.

(3) Nozik, A. J. Photochemical Diodes. *Appl. Phys. Lett.* **1977**, *30* (11), 567−569.

(4) Khaselev, O.; Turner, J. A. A Monolithic Photovoltaic-photoelectrochemical Device for Hydrogen Production via Water Splitting. *Science* **1998**, *280* (5362), 425−427.

(5) Sato, S.; Arai, T.; Morikawa, T.; Uemura, K.; Suzuki, T. M.; Tanaka, H.; Kajino, T. Selective CO_2 Conversion to Formate

Conjugated with H_2O Oxidation Utilizing Semiconductor/Complex Hybrid Photocatalysts. *J. Am. Chem. Soc.* **2011**, *133* (39), 15240−3.
(6) Lin, Y.; Xu, Y.; Mayer, M. T.; Simpson, Z. I.; McMahon, G.; Zhou, S.; Wang, D. Growth of *p*-Type Hematite by Atomic Layer Deposition and Its Utilization for Improved Solar Water Splitting. *J. Am. Chem. Soc.* **2012**, *134* (12), 5508−5511.
(7) Chen, Y.; Crittenden, J. C.; Hackney, S.; Sutter, L.; Hand, D. W. Preparation of a Novel TiO_2-Based *p*−*n* Junction Nanotube Photocatalyst. *Environ. Sci. Technol.* **2005**, *39* (5), 1201−1208.
(8) Ida, S.; Takashiba, A.; Koga, S.; Hagiwara, H.; Ishihara, T. Potential Gradient and Photocatalytic Activity of an Ultrathin *p*-*n* Junction Surface Prepared with Two-Dimensional Semiconducting Nanocrystals. *J. Am. Chem. Soc.* **2014**, *136* (5), 1872−8.
(9) Meng, F.; Li, J.; Cushing, S. K.; Zhi, M.; Wu, N. Solar Hydrogen Generation by Nanoscale *p*−*n* Junction of *p*-type Molybdenum Disulfide/*n*-type Nitrogen-Doped Reduced Graphene Oxide. *J. Am. Chem. Soc.* **2013**, *135* (28), 10286−10289.
(10) Matsumoto, Y.; Obata, M.; Hombo, J. Photocatalytic Reduction of Carbon-dioxide on *p*-type $CaFe_2O_4$ Powder. *J. Phys. Chem.* **1994**, *98* (11), 2950−2951.
(11) Ida, S.; Yamada, K.; Matsunaga, T.; Hagiwara, H.; Matsumoto, Y.; Ishihara, T. Preparation of *p*-Type $CaFe_2O_4$ Photocathodes for Producing Hydrogen from Water. *J. Am. Chem. Soc.* **2010**, *132* (49), 17343−17345.
(12) Kim, E. S.; Nishimura, N.; Magesh, G.; Kim, J. Y.; Jang, J. W.; Jun, H.; Kubota, J.; Domen, K.; Lee, J. S. Fabrication of $CaFe_2O_4$/TaON Heterojunction Photoanode for Photoelectrochemical Water Oxidation. *J. Am. Chem. Soc.* **2013**, *135* (14), 5375−5383.
(13) Miyauchi, M.; Nukui, Y.; Atarashi, D.; Sakai, E. Selective Growth of *n*-Type Nanoparticles on *p*-Type Semiconductors for Z-Scheme Photocatalysis. *ACS Appl. Mater. Interfaces* **2013**, *5* (19), 9770−9776.
(14) Liu, Z.; Miyauchi, M. Visible-light Induced Superhydrophilicity on a WO_3/ITO/$CaFe_2O_4$ Heterojunction Thin Film. *Chem. Commun.* **2009**, *15*, 2002−2004.
(15) Matsumoto, Y.; Sugiyama, K.; Sato, E. I. Improvement of $CaFe_2O_4$ Photocathode by Doping with Na and Mg. *J. Solid State Chem.* **1988**, *74* (1), 117−125.
(16) Iwashina, K.; Kudo, A. Rh-Doped $SrTiO_3$ Photocatalyst Electrode Showing Cathodic Photocurrent for Water Splitting under Visible-Light Irradiation. *J. Am. Chem. Soc.* **2011**, *133* (34), 13272−13275.
(17) Torimoto, T.; Horibe, H.; Kameyama, T.; Okazaki, K.; Ikeda, S.; Matsumura, M.; Ishikawa, A.; Ishihara, H. Plasmon-Enhanced Photocatalytic Activity of Cadmium Sulfide Nanoparticle Immobilized on Silica-Coated Gold Particles. *J. Phys. Chem. Lett.* **2011**, *2* (16), 2057−2062.
(18) Nonaka, T.; Dohmae, K.; Araki, T.; Hayashi, Y.; Hirose, Y.; Uruga, T.; Yamazaki, H.; Mochizuki, T.; Tanida, H.; Goto, S. Quick-scanning X-ray Absorption Spectroscopy System with a Servo-motor-driven Channel-cut Monochromator with a Temporal Resolution of 10 ms. *Rev. Sci. Instrum.* **2012**, *83* (8), 5.
(19) Hill, P. M.; Peiser, H. S.; Rait, J. R. The Crystal Structure of Calcium Ferrite and β Calcium Chromite. *Acta Crystallogr.* **1956**, *9* (12), 981−986.
(20) Matsumoto, Y. Energy Positions of Oxide Semiconductors and Photocatalysis with Iron Complex Oxides. *J. Solid State Chem.* **1996**, *126* (2), 227−234.
(21) Obata, K.; Obukuro, Y.; Matsushima, S.; Nakamura, H.; Arai, M.; Kobayashi, K. Electronic Structure of $CaFe_2O_4$ with Antiferromagnetic Spin Ordering. *J. Ceram. Soc. Jpn.* **2013**, *121* (1417), 766−769.